ELSEVIER

Catalysis Today 31 (1996) 45–56

CATALYSIS TODAY

Shape-selective hydrogenation of naphthalene over zeolite-supported Pt and Pd catalysts

Andrew D. Schmitz, Grainne Bowers, Chunshan Song *

Department of Materials Science and Engineering, Fuel Science Program, 209 Academic Projects Building, Pennsylvania State University, University Park, PA 16802, USA

Abstract

Zeolite-supported Pt and Pd catalysts were used to effect naphthalene hydrogenation with high *trans/cis* decahydronaphthalene (DeHN) isomer selectivity. Four zeolites were studied: three hydrogen-mordenites (HM) with different SiO_2/Al_2O_3 ratios (17, 21 and 38) and HY (SiO_2/Al_2O_3 of 5.0). Catalytic selectivity was found to depend on both the metal and the zeolite. Consequently, the catalyst composition could be tailored for selective production of either *cis*-DeHN or *trans*-DeHN. For example, Pt/HY showed especially high selectivity (80%) for *cis*-DeHN and unlike all other catalysts tested, did not promote the isomerization of *cis*-DeHN. On the other hand, equilibrium between the DeHN isomers was achieved with Pd/HM21, giving ca. 93% *trans*-DeHN at 200°C. In general, Pd catalysts showed higher initial selectivity for *trans*-DeHN than Pt catalysts. Also, the isomerization of *cis*-DeHN to *trans*-DeHN was more rapid on Pd catalysts. Selectivity for *trans*-DeHN increased with the fraction of weak acid sites on the zeolite (measured gravimetrically, using TPD of *n*-butylamine). No correlation between metal crystallite sizes (determined from XRD line-broadening) and DeHN isomer selectivity was found.

Keywords: Naphthalene; Hydrogenation; Shape-selectivity

1. Introduction

Two configurational isomers of decahydronaphthalene (DeHN) result from per-hydrogenation of naphthalene: *cis* and *trans*. Commercial DeHN solvents manufactured using conventional hydrogenation catalysts generally are a 50/50 mixture of both DeHN isomers. However, there are important applications for the individual isomers, calling for the need to produce them separately. *cis*-DeHN can be used to produce sebacic acid which, in turn, can be used in the manufacture of Nylon 6,10 and softeners. On the other hand, Song et al. have shown that *trans*-DeHN has higher thermal stability than *cis*-DeHN, making it a desirable component in high-Mach jet aircraft fuels where the fuel is exposed to high temperatures [1]. Adding *trans*-DeHN to jet fuels can significantly retard the rates of fuel degradation and carbon deposition at 450°C [2]. Therefore, selective production of either DeHN isomer has its own merits for certain applications.

In the present work, we attempted selective

* Corresponding author. Fax. (+1-814) 8653075, e-mail csong@psu.edu

PII S0920-5861(96)00033-8

naphthalene hydrogenation using zeolite-supported Pt and Pd catalysts. Two types of zeolites were chosen: H-mordenite (HM) and HY. Mordenite has a two-dimensional channel structure with elliptically shaped channels of diameter 6.7×7.0 Å. Since the critical diameter of naphthalene is very close to the HM channel dimension, it was anticipated that naphthalene hydrogenation occurring in the channels would be subject to shape selectivity. HY has large cavities in its interior and narrow channel openings. A reactant that has entered the channel structure may reorient itself and react at catalyst sites on the walls of the cavities. However, because of restricted diffusion at the channel openings, only molecules of appropriate diameter would be produced at an appreciable rate. Again, there is the opportunity for shape-selectivity.

The results of this work showed that the *trans*-DeHN/*cis*-DeHN ratio (*trans*/*cis* ratio) in the product is not a simple function of zeolite pore structure. Other factors were found important such as the concentration of acid sites on the zeolite support, and the choice of the noble metal (Pt or Pd). We will discuss the interplay of these and other parameters as they have been found to affect DeHN isomer selectivity.

2. Experimental

2.1. Catalyst preparation

Eight catalysts were prepared by incipient wetness impregnation of the four NH_4-form zeolites (see Table 1, used as received) by either aqueous $H_2PtCl_6 \cdot xH_2O$ (Aldrich, 99.995% Pt, metal basis) or $PdCl_2$ (Aldrich, 99.999% Pd, metal basis) dissolved in dilute hydrochloric acid (sufficient to form soluble $PdCl_4^{2-}$) to a nominal metal concentration of 6 wt%. Following drying in vacuo, the catalysts were calcined in air at 450°C for 2 h. Metal reduction was done in situ during naphthalene hydrogenation tests under the high-pressure of hydrogen.

2.2. Catalyst evaluation

Catalyst tests were done in a 30 cm^3 stainless-steel microautoclave reactor. The reactor is tee-shaped with most of the reactor internal volume in the horizontal member that contains the catalyst and reactants. The horizontal member is connected by a 10″ length of 1/4″ o.d. tubing to a pressure gauge and valve. Unless otherwise specified, the reactor was charged with 0.4 g catalyst, 1.0 g (7.8 mmol) naphthalene (Aldrich, 99%), 4.0 g *n*-tridecane reaction solvent, and 0.35 g *n*-nonane internal standard. The charged reactor was flushed with H_2, then pressurized to 1500 psig cold (ca. 0.2 g) to start the test. Naphthalene undergoes hydrogenation, even at room temperature, so a consistent procedure was established to minimize the time between reactor pressurization and the start of the run.

The reactor was mounted on a holder and immersed in a fluidized sand bath heater. Mixing was accomplished by vertically agitating the reactor at 240 min^{-1}, with a 1 cm stroke. Naphthalene hydrogenation was studied at 25,

Table 1
Properties of the zeolite starting materials

Zeolite [a]	Zeolite Type	Supplier	SiO_2/Al_2O_3 (mol)	Na_2O (wt%)	Surface area (m^2/g)
HY	zeolite Y	Linde LZ-Y62	5.0	2.5	948
HM17	mordenite	Linde LZ-M-8	17.0	0.05	480
HM21	mordenite	PQ Corp., Inc. CBV 20A	21.1	0.02	606
HM38	mordenite	PQ Corp., Inc. CBV 30A	37.5	0.07	512

[a] Trailing digits specify H-mordenite (HM) SiO_2/Al_2O_3 mol ratio.

100 or 200°C with reaction times from 6 min to 24 h. At the end of the test, the reaction was quenched by immersing the reactor in cold water. After cooling, the gas headspace was collected for analysis and the reactor was opened. The contents of the reactor were then washed with acetone onto a filter, and the solid was dried for XRD examination. Solution products were analyzed by GC-MS and GC-FID. For both GC instruments, the column was 30 m × 0.25 mm DB-17 (J&W Scientific), and the oven temperature program was 100–280°C at 15°C/min.

X-ray powder diffraction analyses (XRD) were done on a Scintag 3100 diffractometer using Cu K_α radiation and a scan rate of 1°2θ/min with 0.02° steps. Metal (111) diffraction lines were profile-fitted assuming peak shapes intermediate between Gaussian and Cauchy. Corrections for $K\alpha_2$-doublet broadening and low-angle reflections were done to extract the pure-line profiles as described elsewhere [3]. Metal crystallite sizes were calculated using the Scherrer equation (wavelength 1.54056 Å, Scherrer constant 0.89) [3]. Silicon powder (−325 mesh) was used as an external standard for measuring instrumental and spectral broadening.

Zeolite acidity characteristics were examined by temperature-programmed desorption of *n*-butylamine (*n*-$BuNH_2$) by methods similar to those reported by Ghosh and Curthoys [4]. In short, samples were outgassed at 450°C at 10^{-2} torr, for 2 h. After cooling to room temperature, a flowing stream of dry nitrogen saturated with *n*-$BuNH_2$ vapor was applied to achieve equilibrium adsorption. Desorption of *n*-$BuNH_2$ was done on a Mettler TG50 thermobalance with 60 cm^3/min dry nitrogen flow. Approximately 10 mg sample was loaded into an alumina crucible and allowed to stand for 0.5 h in the TGA flowstream at 30°C. Much of the weakly bound *n*-$BuNH_2$ desorbs during this period. Subsequently, the temperature was raised to 700°C at 10°C/min. Weight loss from the empty sample crucible was determined in a blank run. Weight loss due to desorption from the sample was then determined by subtraction.

3. Results and discussion

3.1. Effects of catalyst composition on naphthalene hydrogenation

Results for naphthalene hydrogenation at 200°C for the four Pd/zeolite and four Pt/zeolite catalysts are shown in Table 2. All catalysts were tested at 200°C for 60 min, and additional runs were done with the HM38- and HY-supported catalyst at 6–30 min. The products of naphthalene hydrogenation at 200°C are almost exclusively isomeric DeHNs excepting the 6 min run with Pt/HY where a significant amount of tetrahydronaphthalene (TeHN) is also observed. It should be noted that 6 min is the approximate time required for the interior of the reactor to equilibrate to the reaction (sand bath) temperature. Gas headspace analyses show 5–50

Table 2
Catalyst performance in naphthalene hydrogenation at 200°C

Catalyst [a,b]	Time (min)	% Nap. conv.	Product distribution (mol%)		
			TeHN	Total DeHN	*trans*/*cis* DeHN
Pd/HM17	60	99.9	0.0	100.0	1.84
Pd/HM21	60	100.0	0.0	100.0	3.00
Pd/HM38	15	100.0	0.0	100.0	1.89
	30	100.0	0.0	100.0	2.60
	60	100.0	0.0	100.0	4.42
Pd/HY	6	100.0	0.0	100.0	1.70
	15	100.0	0.0	100.0	1.84
	30	100.0	0.0	100.0	2.22
	60	100.0	0.0	100.0	2.69
Pt/HM17	60	100.0	0.0	100.0	0.58
Pt/HM21	60	100.0	0.0	100.0	0.83
Pt/HM38	15	99.6	0.1	99.9	0.86
	30	100.0	0.0	100.0	1.26
	60	100.0	0.0	100.0	2.34
Pt/HY	6	99.9	48.4	51.6	0.24
	15	100.0	0.3	99.7	0.26
	30	100.0	0.0	100.0	0.26
	60	99.9	2.6	97.4	0.18

[a] 0.40 g catalyst.
[b] Trailing digits specify H-mordenite (HM) SiO_2/Al_2O_3 mol ratio.

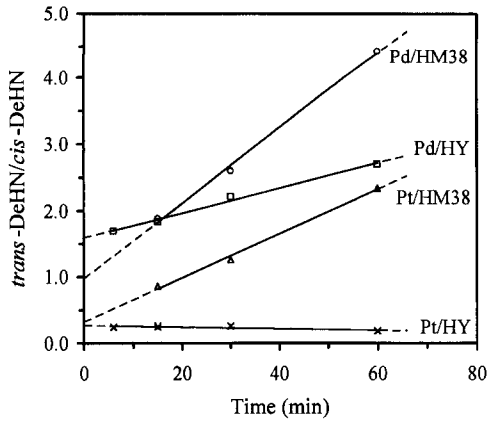

Fig. 1. Temporal variations in the *trans*-DeHN/*cis*-DeHN ratio from naphthalene hydrogenation at 200°C.

ppm levels of C_1–C_4 hydrocarbons. With naphthalene conversion nearly 100% to DeHNs in almost every run, it is not possible to rank catalyst activity. Despite the equivalent conversion levels, it can be seen that the *trans*-DeHN/*cis*-DeHN ratio is highly dependent on both the zeolite and the metal. The HM38-supported catalysts show the greatest potential for selective production of *trans*-DeHN; whereas, the HY-supported catalysts show a striking difference in their DeHN isomer selectivities.

Temporal variations in *trans*-DeHN/*cis*-DeHN ratios are plotted in Fig. 1. Approximate initial hydrogenation selectivities were determined by extrapolating linear regression curvefits to time zero. The *trans*/*cis* ratio increases with time for Pd/HY and the HM38-supported catalysts. When all of the naphthalene is completely saturated, the thermodynamically favorable isomerization of *cis*-DeHN to *trans*-DeHN becomes the main reaction. Pt/HY shows uniquely high selectivity for *cis*-DeHN, and unlike the other catalysts in Fig. 1, the *trans*-DeHN/*cis*-DeHN ratio of 0.2–0.3 does not change with time (beyond experimental error). Clearly, Pt/HY does not promote *cis*-DeHN isomerization.

Several observations concerning trends in DeHN isomer selectivity with catalyst composition can now be made by examining both Table 2 and Fig. 1. First, Pd gives higher *trans*-DeHN selectivity than Pt when supported on the same zeolite. Second, for both Pd and Pt catalysts, *trans*-DeHN selectivity increases with HM SiO_2/Al_2O_3 ratio, and is highest for HM38 support. As seen in Fig. 1, initial selectivity for *trans*-DeHN is higher, and the *trans*-DeHN/*cis*-DeHN ratio increases faster for the Pd catalysts than for Pt catalysts. Comparing 60 min runs for HM17- and HM21-supported catalysts (Table 2), the Pd catalysts always show considerably higher *trans*-DeHN selectivity. This is consistent with the trends observed in Fig. 1 and is likely due to pronounced differences in initial hydrogenation selectivities.

3.2. *Effects of temperature and catalyst charge on naphthalene hydrogenation*

Additional tests were done with Pd/HY (Table 3) and Pt/HY (Table 4) using only 0.10 g catalyst charge, first at 200°C, and then at 100°C. Even after decreasing the Pd/HY catalysts charge from 0.40 to 0.10 g, naphthalene is completely hydrogenated within 30 min at 200°C. At 100°C, the reaction tends to stop at TeHN, with a small amount of DeHNs formed in an approximate 1:1 isomer ratio. For Pt/HY (Table 4), decreasing the catalyst charge and decreasing the reaction temperature have no effect on the *trans*/*cis* ratio. Naphthalene reacts sluggishly on Pt/HY at 100°C, but the percent of DeHNs formed on Pt/HY is nearly double that on Pd/HY.

We also examined naphthalene hydrogena-

Table 3
Effects of reaction time and temperature on Pd/HY catalyst performance (0.10 g catalyst charge)

Time (min)	*T* (°C)	% Nap. conv.	Product distribution (mol%)		
			TeHN	Total DeHN	*trans*/*cis* DeHN
30	200	100.0	0.0	100.0	1.85
60	200	100.0	0.0	100.0	2.26
30	100	99.3	95.2	4.8	1.01
60	100	99.0	93.7	6.3	1.10

Table 4
Effects of reaction time and temperature on Pt/HY catalyst performance (0.10 g catalyst charge)

Time (min)	T (°C)	% Nap. conv.	Product distribution (mol%)		
			TeHN	Total DeHN	*trans*/*cis* DeHN
30	200	100.0	14.7	85.3	0.31
60	200	99.9	0.6	99.4	0.31
30	100	3.9	91.1	8.9	0.25
60	100	5.6	87.5	12.5	0.36

tion at room temperature using Pd/HM17 and Pt/HM17 catalysts (Table 5). Our objectives were to determine if naphthalene would react in our system under such mild conditions, and also to further examine the temperature effect on the product distribution. A substantial amount of naphthalene does react after 12 h, more so in the case of Pt/HM17. Pd/HM17 produces almost exclusively TeHN. The *trans*-DeHN/*cis*-DeHN ratios are low since low temperature favors the kinetic product, the *cis*-DeHN isomer. After charge and pressurization of the batch reactor, a certain amount of time is required for leak-testing and connecting the reactor to the agitation system. Since naphthalene reacts at room temperature, a consistent test procedure (from reactor charge to immersion of the reactor in the sand bath) was needed to avoid artifacts in the data.

TeHN in the main product during naphthalene hydrogenation over Pd catalysts at low temperature (see 100°C data in Tables 3 and 5). The unique ability of Pd for stopping naphthalene hydrogenation at TeHN has been well documented by Weitkamp [5]. Weitkamp suggested that naphthalene may either behave as an adsorbed olefin or an adsorbed aromatic as shown below. Palladium will preferentially adsorb and saturate olefins in olefin/aromatic mixtures [5]. It may be that the interaction of naphthalene with Pd is similar to η^2-olefin coordination.

Table 5
Naphthalene hydrogenation over metal-loaded HM17 catalysts in 12 h runs at 25°C

Catalyst [a,b]	% Nap. conv.	Product distribution (mol%)		
		TeHN	Total DeHN	*trans*/*cis* DeHN
Pd/HM17	26.0	99.7	0.3	0.39
Pt/HM17	87.6	92.6	7.4	0.27

[a] 0.40 g catalyst.
[b] Trailing digits specify H-mordenite (HM) SiO_2/Al_2O_3 mol ratio.

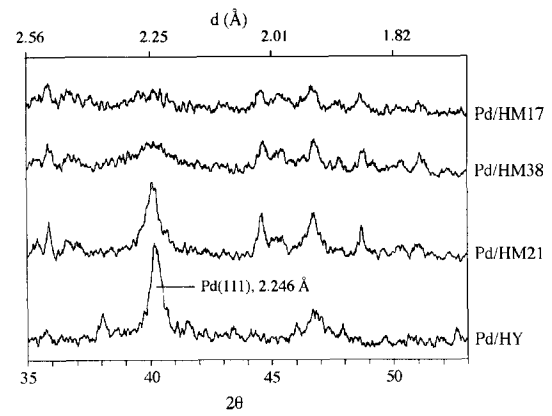

Fig. 2. XRD patterns for palladium catalysts in the region of the Pd(111) and Pd(200) lines.

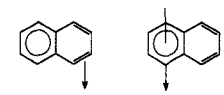

3.3. XRD observations

XRD patterns for catalysts after use in 1 h runs at 200°C are shown in Figs. 2–4. Only

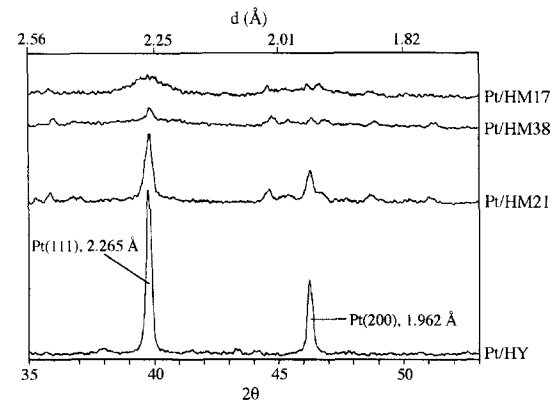

Fig. 3. XRD patterns for platinum catalysts in the region of the Pt(111) and Pt(200) lines.

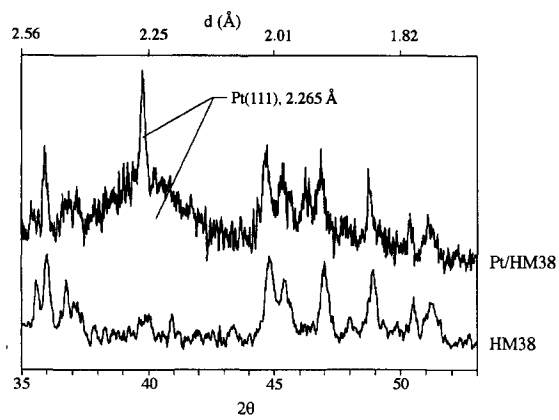

Fig. 4. Region of the Pt(111) in the XRD patterns from Pt/HM38 and HM38. The Pt(111) is composed of a sharp line superimposed on a broad band showing that Pt is bidisperse. Scattering from the HM38 support does not significantly interfere with either Pt(111) signal.

diffraction lines corresponding to the zero-valency state of the metals are observed. Catalysts from the 30 min runs at 200°C also show only the metallic phases. It is apparent that in situ hydrogen treatment effects complete metal reduction. Large differences in diffraction line-widths are seen, especially for the Pt catalysts. Average metal crystallite sizes calculated from the XRD line widths and the Scherrer equation [3] are compared in Table 6. Pt/HY shows very sharp and intense metal diffraction lines, but the band from Pt/HM17 and the major band from Pt/HM38 are very broad (small-particle Pt).

Table 6
Average metal particle sizes determined from XRD line-broadening on catalysts used in 1 runs at 200°C

Catalyst	Average metal particle size (Å)
Pd/HM17	60 [a]
Pd/HM21	310
Pd/HM38	60 [a]
Pd/HY	310
Pt/HM17	120
Pt/HM21	590
Pt/HM38	50 (750) [b]
Pt/HY	1700

[a] Diffuse diffraction line makes accurate width measurement difficult. Particle size estimate reported is approximately the upper limit.
[b] Bidisperse metal. Particle sizes for the broad (and sharp) components of the Pt(111) are indicated.

Fig. 4 shows that the Pt-phase of Pt/HM38 is bidisperse: a sharp line (750 Å Pt) appears superimposed over a very broad band (50 Å Pt). XRD lines for Pd/HM17 and Pd/HM38 (Fig. 2) are very diffuse, making accurate line-width measurements difficult. Conservatively narrow line-width estimates were used to determine crystallite size for these samples.

There is no clear correlation between metal crystallite size and DeHN isomer selectivity. Pd/HM17 and Pd/HM38 have similar metal dispersions, but give very different *trans/cis* ratios. Neither naphthalene hydrogenation nor interconversion of DeHN isomers involves C–C σ-bond breaking. This reaction may be insensitive to metal particle size variations.

3.4. Catalyst acidities

An indicator that zeolite acidity influences the reaction steps where DeHN is formed is the observed sensitivity of the *trans*-DeHN/*cis*-DeHN ratio to HM aluminum content. Thermal gravimetric analysis (TGA) was used to measure catalyst acidities by probing desorption of the base *n*-$BuNH_2$. Two properties of *n*-$BuNH_2$ make it a particularly attractive adsorbate for this study. Unlike smaller adsorbates such as NH_3 or H_2O, diffusion of the larger *n*-$BuNH_2$ molecule in the zeolite micorpores is impeded, much the same as the bicyclic reacting species. Acidity measured with *n*-$BuNH_2$ is therefore representative of the acid sites available to the reacting species during naphthalene hydrogenation. Furthermore, TGA is not a particularly sensitive method for measuring desorption, but sensitivity is enhanced when a relatively high molecular weight adsorbate such as *n*-$BuNH_2$ is used.

TGA *n*-$BuNH_2$ desorption data for the zeolite supports are shown in Fig. 5. Based on these data, zeolite total acidities decreases in the order HY > HM38 ≈ HM21 > HM17. Though HM38 and HM21 acidities are very similar, HM38 shows a larger weight loss in the range 100–340°C, and smaller weight loss above 340°C.

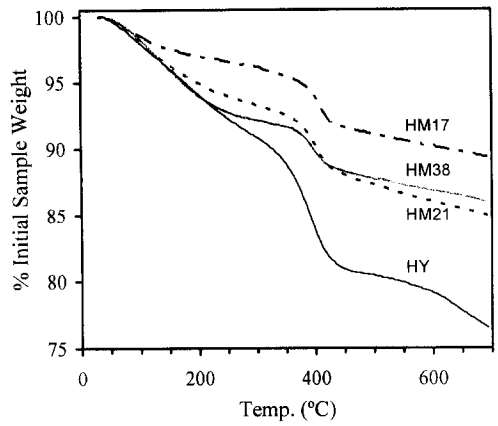

Fig. 5. TGA weight loss curves for n-$BuNH_2$ desorption from the zeolites. Temperature programming: 30 to 700°C at 10°C/min.

The rapid weight losses at 340–500°C are due to the decomposition of n-$BuNH_2$ adsorbed on strong acid sites according to the report by Ghosh and Curthoys [4]. It was proposed that sorbed n-$BuNH_2$ undergoes a Hofmann degradation as shown below [4].

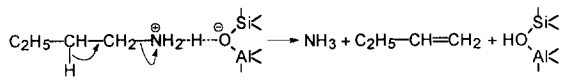

In Table 7, a semi-quantitative tabulation of acid strength is made by defining three regions of relative acid site strength. Weight loss at 100–240°C corresponds to n-$BuNH_2$ desorption from weak acid sites, intermediate at 240–340°C, and strong acid sites at 340–500°C. These temperature regions correspond to three main endothermic features observed in the analysis of n-$BuNH_2$ desorption by differential scanning calorimetry [6]: a low-temperature peak near 100°C, a shallow peak at approximately 200°C, and a large peak at ca. 405°C. Weight loss below 100°C is primarily due to physisorbed n-$BuNH_2$ and is neglected in the determination of zeolite acidity [4]. Also excluded is the weight loss above 500°C which is likely due to zeolite dehydroxylation [4]. It was assumed that butene formed in the Hofmann degradation of n-$BuNH_2$ (340–500°C) desorbs from the catalyst. The amount of n-$BuNH_2$ desorbed is then easily calculated. However, some carbonization of the catalysts occurred, so the determination of strong acid sites is only approximate.

Table 7
Zeolite acidity from desorption of n-$BuNH_2$

n-$BuNH_2$ desorption temp.	Acid site strength	Acidity (mmol/g)			
		HM17	HM21	HM38	HY
100–240°C	weak	0.19	0.56	0.81	0.88
240–340°C	intermediate	0.10	0.18	0.16	0.52
340–500°C	strong	0.57	0.78	0.59	1.50
	Total	0.86	1.52	1.56	2.90

It is clearly seen in Table 7 that HM38 has a higher percentage of weak acid sites than the other two mordenites, and HY has the highest acidity in all three categories. The percentage of acid sites in each of the defined regions is compared in Fig. 6 for the different zeolite supports. This type of data presentation helps to identify a trend: a greater abundance of weak acid sites favors the formation of *trans*-DeHN (compare with the *trans*-DeHN/*cis*-DeHN ratios in). In fact, the correlation is linear for Pd catalysts as shown in Fig. 7. Pt catalysts also show increasing *trans*/*cis* ratio with weak acid sites, but the trend is not linear throughout.

TGA n-$BuNH_2$ desorption data for several metal-loaded zeolites are compared with the parent zeolite supports in Figs. 8 and 9. The

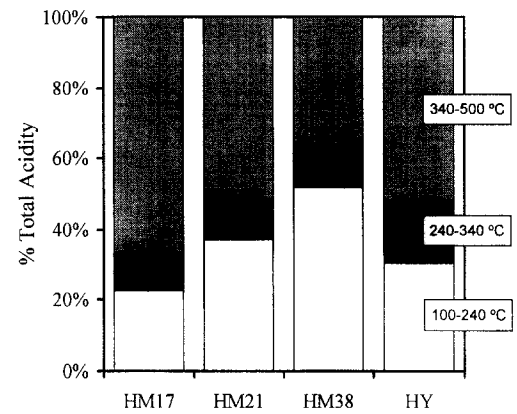

Fig. 6. Acidity distribution plot for the zeolites. Acid site strengths are categorized according to the temperature of n-$BuNH_2$ desorption: weak (desorption at 100–240°C), intermediate (240–340°C), and strong (340–500°C).

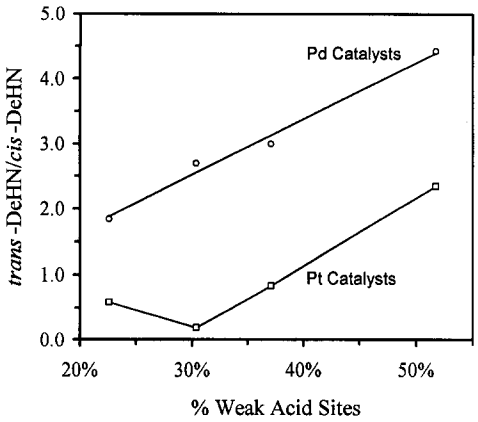

Fig. 7. Correlation between DeHN isomer selectivity and the relative concentration of weak acid sites on the zeolites.

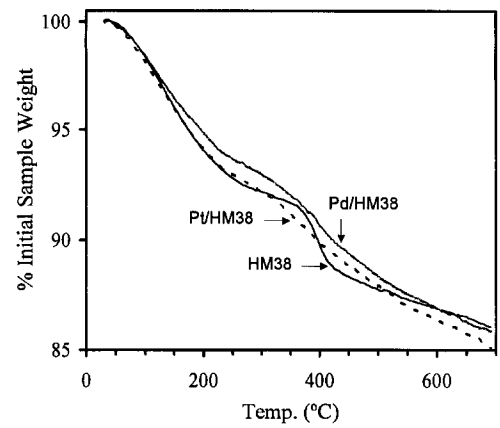

Fig. 9. TGA weight loss curves for n-$BuNH_2$ desorption from HM38 and metal-loaded HM38 catalysts. Temperature programming: 30 to 700°C at 10°C/min.

metal-loaded HY catalysts give nearly linear weight loss curves, devoid of the rapid weight loss at 340–500°C which is so apparent for HY. Apparently, the metals hinder access of n-$BuNH_2$ to the strong acid sites, and desorption occurs without decomposition. One explanation for this behavior is that the metal particles preferentially attach to the support at strong acid centers to neutralize them. Metal-support interactions of this nature may explain why Group VIII metals on acidic zeolites, especially on HY, are known to be electron deficient [7]. A second possibility is that metal particles prevent n-$BuNH_2$ from diffusing to strong acid sites by blocking the channel openings. Micropore diameters for both types of zeolites are less than 8 Å. The large metal particles observed in the XRD must reside on the external surfaces of HY, and a certain number of channel openings will be blocked. However, if channel blockage is the most important factor involved, Pd/HY and Pt/HY might be expected to give dissimilar acidity spectra, because they have very different average metal crystallite sizes. But their acidity spectra are nearly identical. It is also interesting to note that Pt/HY and Pd/HY give very different DeHN isomer selectivities. Apparently, selectivity is largely influenced by metal identity and the shape-selectivity afforded by the zeolite.

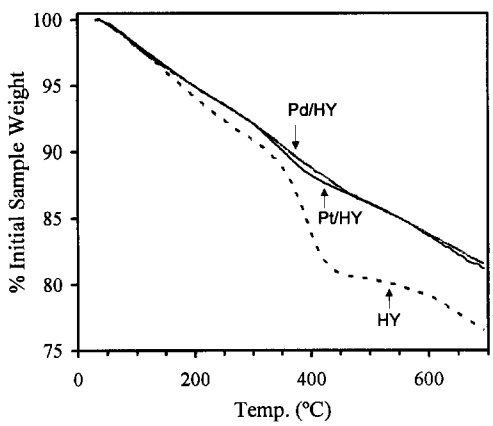

Fig. 8. TGA weight loss curves for n-$BuNH_2$ desorption from HY and metal-loaded HY catalysts. Temperature programming: 30 to 700°C at 10°C/min.

Pd/HM38 and Pt/HM38 give acidity spectra that are similar to each other, and similar to HM38 (Fig. 9). The presence of a metal phase does not significantly impede diffusion of n-$BuNH_2$ since the acidities in Fig. 9 are so similar. XRD shows that the metals are fairly well dispersed on HM38 support. It is possible that a significant portion of the metals reside in the HM side-channels that run perpendicular to the main channels. Such a highly-dispersed phase would be transparent to the XRD, and would not affect diffusion of n-$BuNH_2$ in the main channels.

To summarize, catalyst acidity seems to be an important factor when comparing the same

metal on different zeolite supports. However, catalysts having very similar acidity, such as Pd/HY and Pt/HY, can still give very different DeHN isomer selectivities. Consequently, metal identity and zeolite structure must be very important. Hydrogen addition to naphthalene is likely to be metal centered, but acidic zeolite supports can effect the metal's electronic properties by forming charge-transfer complexes with the metal. Also, shape-selectivity can arise for hydrogenation reactions that occur within the micropores. Some hydrocarbon isomerization reactions occur readily on acidic zeolites. In fact, Lai et al. showed that the HM38 catalyst used in this work catalyzes the isomerization of *cis*-DeHN to *trans*-DeHN and that Pt/HM38 and Pd/HM38, under H_2 environment, were considerably more effective catalysts [8].

3.5. *cis*-DeHN to *trans*-DeHN isomerization at 200°C

With TeHN as an intermediate, naphthalene hydrogenation can be pictured as shown in Scheme 1. Our data show the following relative rate constant values: $k_1 \gg k_2 > k_3 \approx k_4$. In a recent detailed kinetic analysis of naphthalene hydrogenation over Pt/Al_2O_3, Huang and Kang reported that the isomerization of *cis*-DeHN could be treated as irreversible ($k_4 \gg k_{-4}$), and dehydrogenation of DeHN could be neglected [9]. Therefore, when naphthalene conversion to DeHNs is complete, the rate expression for the isomerization is a simple expression involving only the *cis*-DeHN concentration. This simplification does not hold when the TeHN concentration is non-zero.

Plots of log *cis*-DeHN concentration vs. time

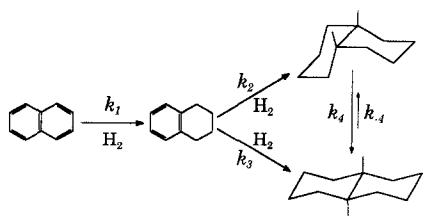

Scheme 1. Reaction pathway for naphthalene hydrogenation.

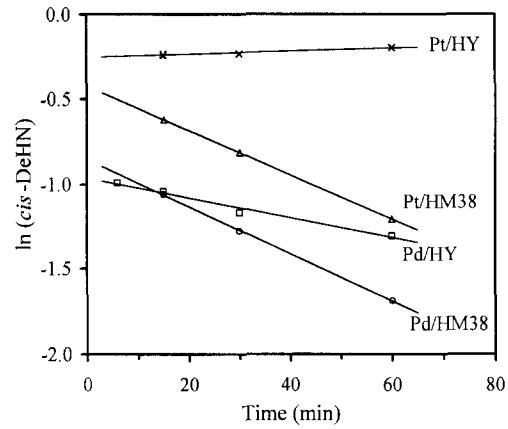

Fig. 10. First-order rate constant plots for *cis*-DeHN to *trans*-DeHN isomerization at 200°C.

using the data from Table 2 are linear (Fig. 10) showing that the isomerization of *cis*-DeHN is first-order. Values determined for k_4 are compared in Table 8 together with some values collected from the literature. Not only does Pd/HM38 have a higher initial selectivity for *trans*-DeHN, but it also isomerizes *cis*-DeHN faster than Pt/HM38. Pd/HY gives a value of k_4 that is approximately one-half the values obtained for HM38-supported catalysts; k_4 for Pt/HY is zero.

Huang and Kang measured the *cis*-DeHN isomerization rate constant for direct *cis*-DeHN isomerization and for isomerization occurring

Table 8
Comparison of *cis*-DeHN isomerization rate constants from this work and the literature

Catalyst	k_4 (h^{-1})	k_4 (mmol/g cat h)
Pd/HY	0.35	6.9
Pt/HM38	0.78	15.2
Pd/HM38	0.84	16.4
Pt/HM38 [a]	0.30	10.9
Pd/HM38 [a]	0.30	10.8
Pt/Al_2O_3 [b]	0.11	na
Pt/Al_2O_3 [c]	5.4 (0.45)	na

[a] Reaction of a 50:50 mixture *cis*- and *trans*-DeHN at 200°C and 100 psi H_2 from Ref. [8].
[b] Naphthalene hydrogenation at 200°C and 750 psi from Ref. [9]; na, not available.
[c] Isomerization of *cis*-DeHN at 220°C and 750 psi from Ref. [9]; value in parenthesis calculated for reaction at 200°C using reported activation energy, 19.8 kcal/mol.

during naphthalene hydrogenation [9]. They did not report the mass of catalyst used, so a comparison of specific rate constants can not be made. Their value from direct *cis*-DeHN isomerization is comparable to our values, but their value of 0.11 h^{-1} measured during naphthalene hydrogenation is low. Higher acidity of the zeolites, compared to Al_2O_3 support, may account for our higher isomerization activities. We have already shown (Fig. 7) that the *trans*-DeHN/*cis*-DeHN ratio increases with acid site density.

To explain differences in the isomerization rate constant for the different processes, Huang and Kang proposed that naphthalene and TeHN compete with *cis*-DeHN for adsorption on catalyst sites during naphthalene hydrogenation and reduce the *cis*-DeHN isomerization rate [9]. Significant differences in the *trans*/*cis* ratio and the *cis*-DeHN isomerization rate constant were also reported in other work on the hydrogenation of naphthalene or TeHN [5,10].

Lai and Song used the same Pd/HM38 and Pt/HM38 catalysts as used here to measure the *cis*-DeHN isomerization rate at 200°C, starting from a 1:1 mixture of *cis*- and *trans*-DeHN [8]. Their rate constants are smaller than those of the present work which may be the result of a lower H_2 pressure (100 psi). Lai and Song also compared *cis*-DeHN isomerization under nitrogen and hydrogen. They found that *cis*-DeHN isomerization is much faster under H_2. An earlier report by Petrov et al. showed that nickel can catalyze the isomerization of *cis*-DeHN, but only in the presence of H_2 [11]. These results indicate that the main *cis*-DeHN isomerization pathway is metal-centered for zeolite-supported metal catalysts.

In order to determine the practical equilibrium *trans*-DeHN/*cis*-DeHN ratio under hydrogenation conditions, four tests were done with Pd/HM21 at extended reaction times (Table 9). An approximately constant *trans*/*cis* ratio of 13.6 is obtained within 6 h reaction time. This value is somewhat lower than the calculated equilibrium constant for *cis*-DeHN to *trans*-DeHN isomerization of 20.5 at 200°C [8]. However, we have confirmed that the practical limit is ca. 14 using other Pt/zeolite and Pd/zeolite catalysts. Some DeHN may reside in the portion of the reactor that extends above the sand level in the fluidized sand bath, the cold zone, and may not react. According to calculations, even if 5% of the DeHN does not react to form an equilibrium amount of *trans*-DeHN, the equilibrium constant value falls to 13.0 [8].

Table 9
Equilibrium DeHN isomer distribution from naphthalene hydrogenation over Pd/HM21 at 200°C [a]

Time (h)	% Nap. conv.	Product distribution (mol%)		
		TeHN	Total DeHN	*trans*/*cis* DeHN
1	100.0	0.0	100.0	3.26
6	100.0	0.0	100.0	13.46
10	100.0	0.0	100.0	13.74
24	100.0	0.0	100.0	13.59

[a] 0.40 catalyst.

3.6. Mechanism of selective DeHN isomer production

There is clearly a correlation between *trans*-DeHN selectivity and zeolite acidity for the different catalysts. The implication is that at least one of the reactions which govern selectivity are sensitive to the zeolite structure and/or makeup. On the other hand, zeolite-supported catalysts with very similar acidity can give very different *trans*-DeHN/*cis*-DeHN ratios (cf. Pd/HY and Pt/HY). To understand the catalyst properties that govern selectivity, it is necessary to understand the mechanism by which *trans*/*cis* orientation is determined.

Weitkamp showed that DeHN *trans*/*cis* orientation is determined in the hydrogenation of $\Delta^{9,10}$-octahydronaphthalene **1** ($\Delta^{9,10}$-OHN) and $\Delta^{1,9}$-OHN **2** intermediates during naphthalene hydrogenation [5]. Other partially hydrogenated products do not play a direct role in determining DeHN *trans*/*cis* configuration. Weitkamp also showed that hydrogen addition to a cyclic olefin is always *syn* [5]. Likewise, molecular metal

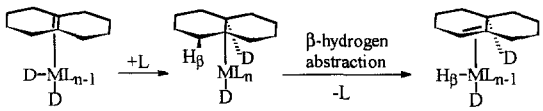

Scheme 2. Proposed mechanism for $\Delta^{9,10}$-OHN isomerization on a metal complex. Adapted from Ref. [5].

catalysts give only *syn*-addition of hydrogen as demonstrated by Stuhl et al. who used η^3-$C_3H_5Co[P(OCH_3)_3]_3$ precatalyst to hydrogenate naphthalene with 100% conversion to 99% *cis*-DeHN and 1% TeHN [12]. Consequently, coordination of **1** to a metal atom with subsequent *syn*-addition of hydrogen, and no olefin isomerization, can only result in the formation of *cis*-DeHN [5]. In fact, Weitkamp showed by deuteration of **1** and **2** over heterogeneous Pt catalysts that dideuterium addition across the $\Delta^{9,10}$-olefin only occurs *syn* [5]. Any *trans*-DeHN formed from **1** had deuterium incorporation d_3, not just d_2, due to prior isomerization of **1** to **2** as shown in Scheme 2. The second step in Scheme 2, abstraction of a β-hydrogen, results in coordinated $\Delta^{1,9}$-OHN. This coordinated olefin may remain adsorbed and undergo deuteration, forming d_3 *cis*-DeHN. Or, it may dissociate from the metal (i.e. desorb from the catalyst surface). Readsorption of **2** can occur in two ways: deuterium down or deuterium up. Deuteration then gives either *cis*-DeHN-d_3, or *trans*-DeHN-d_3, respectively. Platinum, rhodium, iridium and especially ruthenium favor *cis*-adsorption of **2** (metal and bridgehead deuterium on the same face as shown in Scheme 2) and produce mostly *cis*-DeHN; other metals, especially palladium, favor *trans*-adsorption leading to *trans*-DeHN [5].

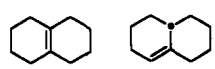

1 2

Compared to Pd on the same zeolite, Pt always gives a higher initial *cis*-DeHN selectivity, Pt isomerizes *cis*-DeHN more slowly, and Pt has lower activity (compare naphthalene conversions at 100°C). These differences may be tied to the bond strength between the metal and olefins **1** and **2**. This argument may be especially important for HY-supported catalysts, since Group VIII metals on acidic zeolites, especially on HY, are known to be electron deficient [7]. Olefin adsorption on an electron deficient metal would be comparatively strong due to electron density transfer from the olefin to the metal (σ-donation). Formation of *trans*-DeHN requires that **2** desorb from the surface of the catalyst, rotate, and undergo *trans* adsorption. If this key OHN intermediate is strongly bound on electron deficient Pt, its desorption prior to hydrogenation is unlikely. Its most probable course of reaction is hydrogenation to *cis*-DeHN, but since it is strongly bound, even hydrogenation occurs slowly. It follows that k_2/k_3 will be larger for Pt/zeolite, and since **2** is also an intermediate in *cis*-DeHN isomerization, k_4 will be smaller for Pt/zeolite. If the olefin–metal bond strength argument applies, Pt on HY is extremely electron deficient. A comparative IR investigation of CO or NO adsorption states could give the necessary information about the electronic states of the metals. Both of the adsorbates have vibrations that are sensitive to the electron density about the metal.

Is it a coincidence that Pt/HY has the largest metal particle size (1700 Å average diameter) of all the catalysts? Metal-support interactions are generally unimportant for large particles; significant effects on metal particle shape and electronic properties are generally only noted for very small metal particles (i.e. < 50 Å diameter). It may be that *cis*-DeHN is produced on highly dispersed Pt that is XRD transparent and located in the confines of the HY major pore structure. Large-particle Pt has proportionately much lower surface area and resides on the external surfaces of the catalyst. Naphthalene and its hydrogenated products, however, are concentrated in the catalyst particles interior. A second possibility with large Pt particles on the external surface of the catalyst is partial channel-opening blockage which could give rise to

shape-selectivity. The problem with both of these explanations – bidisperse Pt or partial channel blockage – is that neither accounts for the lack of *cis*-DeHN isomerization over time. There must be some non-selective active sites on the external surface of the catalyst, and these sites should effect the isomerization. Electron microscopy and hydrogen chemisorption could be used to reevaluate metal particle dispersion in attempt to answer these questions.

4. Conclusions

It has been established that the naphthalene hydrogenation process can be tailored to produce either *cis*-DeHN or *trans*-DeHN by appropriate choice of the zeolite and metal species. Selectivity for *trans*-DeHN increases with SiO_2/Al_2O_3 ratio in the HM catalysts. This trend is parallel to an increasing percentage of weak acid sites with SiO_2/Al_2O_3 ratio. Compared to Pt on a given zeolite, Pd shows a higher initial selectivity for *trans*-DeHN, and a higher rate for *cis*-DeHN to *trans*-DeHN isomerization. The practical equilibrium *trans/cis* ratio is 14 at 200°C. Metal crystallite sizes are highly dependent on the zeolite. Pd generally had a higher dispersion than did Pt on a given zeolite. Naphthalene hydrogenation and *cis*-DeHN isomerization may be structure insensitive reactions. DeHN isomer selectivity does not show a correlation with particle size. Pt/HY gives high selectivity for *cis*-DeHN and does not promote *cis*-DeHN isomerization. We offer three possible explanations for this unique selectivity: (1) lack of isomerization of olefin intermediates due to strong bonding on electron deficient Pt particles, (2) partial channel blockage by the large Pt particles giving rise to a unique type of shape-selectivity, or (3) bidisperse Pt with most of the reaction occurring on small Pt particles within the shape-selective channel structure of HY. Further study will be needed to clarify the origin of the selectivity differences.

Acknowledgements

We wish to thank the following persons at the Pennsylvania State University: Professor Harold Schobert for his encouragement and support, and Dr. W.-C. Lai for performing *n*-$BuNH_2$ desorption experiments on Pd/HM38 and Pt/HM38 and his thoughtful comments on this work. This work was jointly supported by the US Department of Energy, Pittsburgh Energy Technology Center, and the Air Force Wright Laboratory. We would also like to thank Mr. W.E. Harrison III of USAF and Dr. S. Rogers of DOE for their support.

References

[1] C. Song, S. Eser, H.H. Schobert and P.G. Hatcher, Energy Fuels, 7 (1993) 234.
[2] C. Song, W.-C. Lai and H.H. Schobert, Am. Chem. Soc. Div. Fuel Chem. Prepr., 37 (1992) 1655.
[3] H.P. Klug and L.E. Alexander, X-ray Diffraction Procedures for Polycrystalline and Amorphous Materials, Wiley, New York, 1974, see example calculations on p. 699.
[4] A.K. Ghosh and G. Curthoys, J. Phys. Chem., 88 (1984) 1130.
[5] A.W. Weitkamp, Adv. Catal., 18 (1968) 1.
[6] C. Song, W.-C. Lai A.D. Schmitz and K.M. Reddy, Am. Chem. Soc. Div. Fuel Chem. Prepr., 41 (1) (1996) 71.
[7] A. Stanislaus and B.H. Cooper, Catal. Rev., Sci. Eng., 36 (1994) 75.
[8] W.-C. Lai and C. Song, Am. Chem. Soc. Div. Fuel Chem. Prepr., 40(4) (1995) 1018.
[9] T.-C. Huang and B.-C. Kang, Ind. Eng. Chem. Res., 34 (1995) 1140. The authors neglected to divide the slopes from activation energy plots by the gas constant (1.987 cal/mol K) for reporting activation energies.
[10] S.C. Korre, M.T. Klein and R.J. Quann, Ind. Eng. Chem. Res., 34 (1995) 101.
[11] L. Petrov, L. Angelova and D. Shopov, Bokl. Bolg. Akad. Nauk., 30 (1977) 85.
[12] L.S. Stuhl, M. Rakowski DuBois, F.J. Hirsekorn, J.R. Bleeke, A.E. Stevens and E.L. Muetterties, J. Am. Chem. Soc., 100 (1978) 2405.